RSC Advances

PAPER

View Article Online
View Journal | View Issue



Cite this: *RSC Adv.*, 2021, **11**, 35842

# Novel copper sulfide doped titania nanoparticles as a robust fiber coating for solid-phase microextraction for determination of polycyclic aromatic hydrocarbons†

Mingguang Ma, Yunxia Wei* and Fang Liu

Immobilized $TiO_2$ nanoparticles modified by nanoscale CuS (CuS@$TiO_2$NPs) were successfully synthesized and used as fibers for solid-phase microextraction (SPME) for the determination of some polycyclic aromatic hydrocarbons (PAHs) in water samples. A novel fiber has been developed by postprecipitation of CuS coated the titania nanoparticles *in situ* grown on a titanium wire annealed at 550 °C in a nitrogen ambient atmosphere. Its morphology and surface properties were characterized by scanning electron microscopy and energy dispersive X-ray spectrometry. It was connected to high performance liquid chromatography-ultraviolet detector (HPLC-UV) equipment by replacing the sample loop of a six-port injection valve, building the online SPME-HPLC-UV system. Variables affecting extraction procedures, including desorption time, stirring speed, extraction temperature, extraction time and ionic strength were investigated and the parameters were optimized. The SPME fiber exhibits high selectivity for the five PAHs studied. The linear ranges varied between 0.15 μg $L^{-1}$ and 200 μg $L^{-1}$ with correlation coefficients ranging from 0.9913 to 0.9985. LODs and LOQs ranged from 0.02–0.04 μg $L^{-1}$ and 0.07–0.13 μg $L^{-1}$. RSDs for one fiber and fiber-to-fiber were in the range of 3.2–4.3% and 4.6–6.8%, respectively. Additionally, the fiber possessed advantages such as resistance to organic solvent, high mechanical strength and difficult breakage, making it have strong potential applications in the selective extraction of PAHs from complex water samples at trace levels.

Received 6th August 2021
Accepted 31st October 2021

DOI: 10.1039/d1ra05966a

rsc.li/rsc-advances



## 1. Introduction

Solid-phase microextraction (SPME) is distinguished from many extraction techniques because of its advantages such as low cost, high enrichment factor, wide scope, less secondary pollution, rapidness, and removal of the potentially interfering matrix.[1–3] For SPME, fiber nature is no doubt the key to determine its extraction sensitivity, selectivity and reproducibility. Nonetheless, the technique is mainly determined by the properties of the adsorbent coated on the SPME device. Up to now, commercially fibers such polydimethylsiloxane (PDMS), divinylbenzene (DVB), polyacrylate (PA), Carboxen (CAR), polyethylene glycol (PEG) and their composites have successfully developed,[4–6] still there exist a number of shortcomings that need to be overcome. For example, breakage of the fiber, stripping of the coating, relatively low operating temperature, and instability and swelling in organic solvents.[7] To improve its overall extraction performance, a large amount of research relating fiber materials, coating materials and coating procedures have been the focus of related researches.[8–12]

$TiO_2$ as a promising material has gained great interest in analytical chemistry because of its good adsorptivity, durability, high stability, corrosion resistance, and non-toxicity, has been successfully used as the SPME fiber. Especially with the special relatively strong Lewis acidic and basic surface property, $TiO_2$ coatings would hold great prospects to exhibit special selectivity for extracting some compounds.[13–17]

Bulk heterojunctions with three-dimensional nanostructures have attracted tremendous attention in SPME, because of their larger specific surface, diverse chemical design and inexpensive solution-based process.[18–20] To utilize the oriented feature of $TiO_2$ nanoparticles ($TiO_2$NPs), an emerging concept is to modify the nanoparticles with various nanoparticles, and thus forming a heterojunction. Some variety of approaches have been deployed, such as chemical deposition,[21] solvothermal treatment,[22] spotting sample method,[23] chemical precipitation,[24] and electrodeposition.[25] A number of studies focus on filling up the $TiO_2$ nanotubes ($TiO_2$NTs) with various nanoparticles. However, insufficient tube filling is the key problem hindering its further development. This produces a large number of particles isolated from each other and hence

*College of Chemistry and Chemical Engineering, Lanzhou City University, Lanzhou 730070, China. E-mail: weiyx07@lzu.edu.cn*

† Electronic supplementary information (ESI) available. See DOI: 10.1039/d1ra05966a

degrading the material performances.[26,27] It is noteworthy that all of these studies produce bulk heterojunctions by filling up the nanotubes with discrete nanoparticles, where the low filling rate always affects the material properties. A homogeneous nanocomposite films are highly desirable, which exhibit superior performance in terms of large interfacial area for selective extraction of organic compounds. At present, the researchers have successfully combined $TiO_2$ with other nanomaterials to form nanocomposites and applied this material to SPME fiber coating.[28–30] Among these nanometer materials, copper monosulfide (CuS) nanoparticles has drawn an increasing attention due to long-term stability, environmental benignity, large specific surface area and strong hydrophobicity. In the present study, a novel $TiO_2$NPs coating was *in situ* fabricated by direct anodization of Ti wire substrates in ethylene glycol with concentrated $NH_4F$ and it provided a desired nanostructured substrate for subsequent surface modification. The growth of a CuS/$TiO_2$ nanocomposite coating was developed by direct chemical deposition with a Ti wire as a supporting substrate. CuS was synthesized by using a postprecipitation method with sodium sulfide and copper nitrate as sulfur source and copper source respectively.

## 2. Experimental

### 2.1. Chemicals and reagents

Copper nitrate ($Cu(NO_3)_2$) was supplied by Zhanyun Chemical Reagent Co., Ltd (Shanghai, China). Sodium sulfide (NaS) was obtained from Tianjin Beilian Fine Chemicals Industry Co., Ltd. (Tianjin, China). Sodium chloride (NaCl), ammonium fluoride ($NH_4F$) and ethylene glycol were purchased from Sinopharm Chemical Reagent Co., Ltd. (Shanghai, China). The HPLC-grade methanol was purchased from Yuwang Chemical Company (Shandong, China). Certified individual standards of naphthalene (Nap), phenanthrene (Phe), fluoranthene (Flt), pyrene (Pyr) and benzo[*a*]pyrene (B[*a*]p) were purchased from Aldrich (St. Louis, MO, USA). Dimethyl phthalate (DMP), diethyl phthalate (DEP), di-*n*-butyl phthalate (DBP), di-*n*-octyl phthalate (DOP), di-(2-ethylhexyl)phthalate (DEHP), aniline (ANI), 4-methylaniline (4-MA), 4-nitroaniline (4-NA), diphenylamine (DPA), 2-hydroxy-4-methoxy-benzophenone (BP-3), 2-ethylhexyl 4-(*N*,*N*-dimethylamino)benzoate (OD-PABA), 2-ethylhexyl-4-methoxycinnamate (EHMC) were supplied by AccuStandard (New Haven, CT, USA). 2-Ethylhexyl salicylate (EHS) was obtained from Dr. Ehrenstorfer (Augsburg, Germany).

Ti wire ($\Phi$ 250 μm, 99.9% in purity) was obtained from the Alfa Aesar (Ward Hill, MA, USA). A commercial SPME device with several fibers including polydimethylsiloxane (PDMS, 100 μm thickness) and polyacrylate (PA, 85 μm thickness) were obtained from Supelco (Bellefonte, PA, USA). 0.45 μm micropore membrane of polyvinylidene fluoride was supplied by Xingya Purifying Material Factory (Shanghai, China).

### 2.2. Instrumentation

Anodization of Ti wires was performed with a precise WY-3D power supply (Nanjing, China). $TiO_2$ nanoparticles were annealed in air atmosphere at different temperatures in OTF-1200X tubular furnace with a Prog/Controller (Kejing, Hefei, China). The fabricated fibers were characterized by an Ultra Plus microscope (Zeiss, Oberkochen, Germany) with an Aztec-X-80 energy dispersive X-ray spectrometer (Oxford, UK). SPME was carried out in a DF-101S thermostat with controlled temperature and magnetic stirring (Changcheng, Zhengzhou, China). The analyses were carried out on a Waters 600E multi-solvent delivery system (Milford, MA, USA) equipped with a Waters 2487 dual $\lambda$ absorbance detector and a Zorbax Eclipse Plus C 18 column (150 mm × 4.6 mm, 5 μm, Agilent, USA). Chromatographic data was processed with a N2000 workstation (Zhejiang University, China). Desorption was performed in a commercially available SPME-HPLC interface (Supelco, PA, USA). Ultrapure water was obtained from a Sudreli SDLA-B-X water purification system (Chongqing, China).

### 2.3. Preparation of the CuS@$TiO_2$NPs fiber

One end of the Ti wire was rinsed with methanol and ultrapure water in an ultrasonic bath for 5 min, respectively. The $TiO_2$NPs/Ti fiber was prepared by a simple electrochemical anodic oxidation method, which was carried out in a conventional two-electrode configuration at 25 V for 1 h. The Ti wire and Pt sheet was served as the working electrode and the counter electrode, respectively. The solution of ethylene glycol containing ultrapure water ((v/v, 1 : 1)) and $NH_4F$ (0.5 wt%) was used as the electrolyte. The anodization experiments were performed at approximate 25 °C for *in situ* growth of $TiO_2$NPs array on the Ti wire. The anodized segment of the Ti wire was rinsed with ultrapure water and then annealed in a quartz tubular furnace at a heating rate of 5 °C $min^{-1}$ up to the preset temperature and held for 2 h. The fabricated fiber was then allowed to cool in nitrogen stream. CuS was deposited on $TiO_2$NPs by postprecipitation method as follows. The $TiO_2$NPs were first immersed into a $Cu(NO_3)_2$ (1 mM) solution for 10 min, thereafter the fiber dried in vacuum at 90 °C and was washed with ultrapure water, then immersed into $Na_2S$ (1 mM) solution for 10 min followed by another drying and rinsing with ultrapure water. The postprecipitation process was repeated multiple times.

### 2.4. Preparation of sample solutions

Standard stock solutions of PAHs, PAEs, aromatic amines and UV filters were individually prepared in methanol at a concentration of 100 mg $L^{-1}$ for each of the analytes and stored in amber bottles in the dark at 4 °C for use. Working solutions were prepared daily by diluting the stock solution with ultrapure water. Water samples from Yellow River at different sites of Lanzhou section were used as real samples. All water samples were filtered through 0.45 μm micropore membranes and then adjusted to pH 7.0 with phosphate buffer, stored in the refrigerator at 4 °C.

### 2.5. SPME-HPLC procedure

The prepared fiber was equipped into a homemade SPME device which was modification of a 5 μL syringe. Before initial extraction, the CuS@$TiO_2$NPs fiber was conditioned in methanol for 15 min with agitation speed of 600 rpm. All the

extractions were performed in direct-immersion mode with 15 mL aqueous solution in a 20 mL vial by exposing a 1.0 cm length of the fiber to the sample solution. A small magnetic stirrer with a water bath was employed to adjust the rotation speed and the extraction temperature. After the extraction, the fiber was withdrawn into the needle, removed from the sample vial and immediately transferred to SPME-HPLC interface connected with six-port injection valve for static desorption in methanol/water serving as a desorption solvent and then the analytes were introduced to the column. This process was accomplished by simply switching the injection valve from the "load" to "inject" position.

The mixtures of methanol and water of 75/25, 75/25, 70/30 and 90/10 (v/v) were employed as mobile phases for HPLC analyses of aromatic amines, Phthalic Acid Esters (PAEs), UV filters and polycyclic aromatic hydrocarbons (PAHs) at a flow rate of 1 mL $min^{-1}$, respectively. The corresponding chromatographic signals were monitored at 284 nm, 280 nm, 305 nm and 254 nm. Between the extractions, possible carryover effect was minimized by immersing the fiber into methanol and ultrapure water for 15 min and 10 min, respectively.

## 3. Results and discussion

### 3.1. Effect of oxidation time

The physical morphology of $TiO_2$NPs has a direct influence on the effect of CuS doping, which further affects the extraction behavior of fiber coating. The oxidation time is a decisive factor

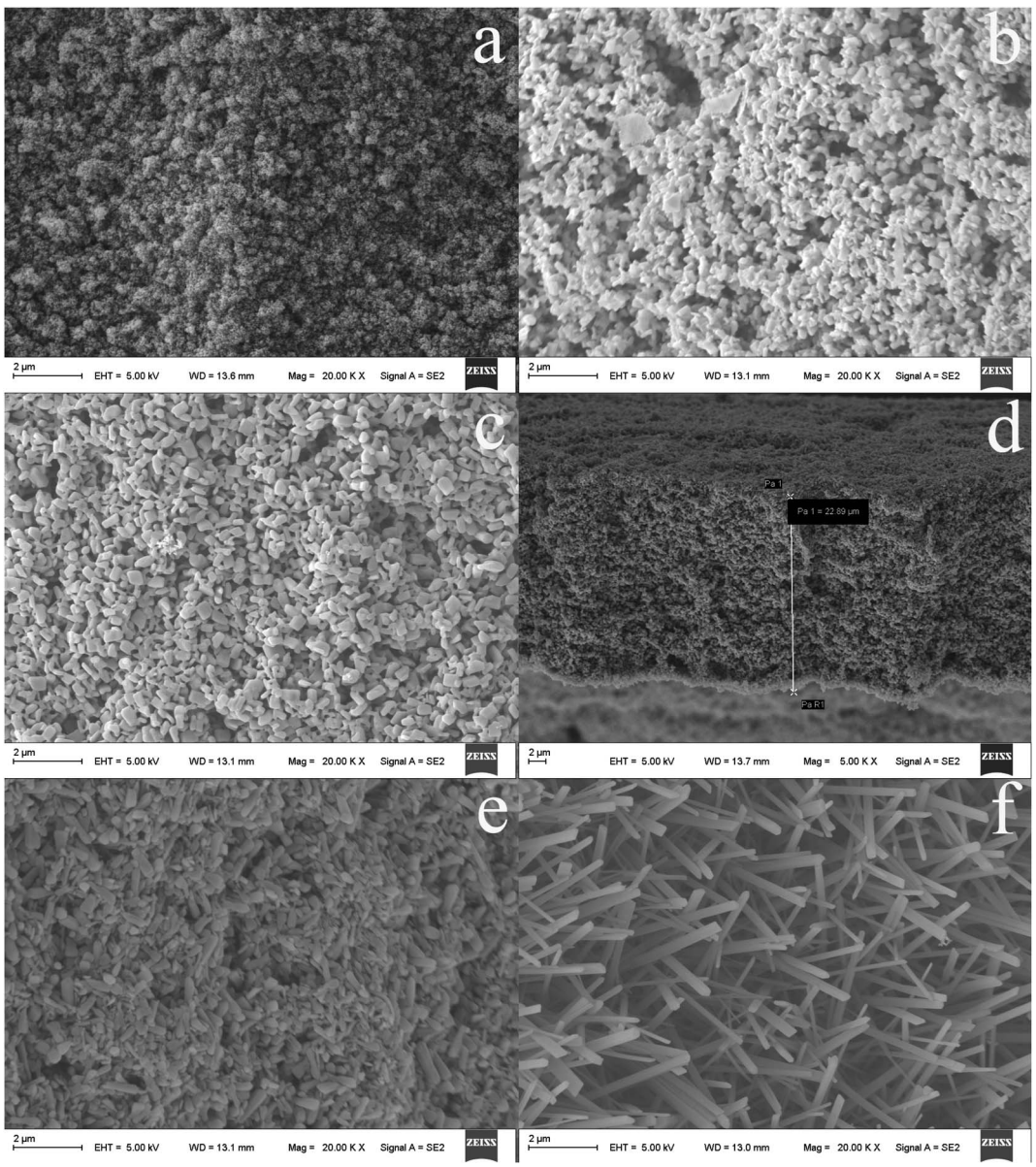


Fig. 1 SEM micrographs of the as-fabricated fiber by anodization within 20 min (a), 40 min (b), 60 min (c), 80 min (e), 100 min (f) and the thickness of $TiO_2$NPs within 60 min of anodization (d).

 

in the formation of fiber coating morphologies. For this purpose, effect of anodic oxide time on $TiO_2$NPs coatings was further examined in electrolyte at 25 V for different time at room temperature for *in situ* growth of $TiO_2$NPs on the Ti wire. As shown in Fig. 1, the $TiO_2$NPs with different morphology were obtained within 20 min (Fig. 1a), 40 min (Fig. 1b), 60 min (Fig. 1c), 80 min (Fig. 1e) and 100 min (Fig. 1f), respectively. As can be seen from Fig. 1, the length of $TiO_2$NPs increases with the prolongation of oxidation time, the nanoparticles thickness, however, changed thinner overall. Proper length of nanoparticles could increase the specific surface of the fibers, but too long length will inevitably lead to a decrease in strength, which is not conducive to further modification of $TiO_2$NPs. This result suggests that $TiO_2$NPs should significantly increase available surface area of the as-fabricated fiber and thereby enhance its the ability of doping copper sulfide. Thus, 60 min was employed as a reasonable compromise between good mechanical strength and suitable specific surface area for the *in situ* fabrication of $TiO_2$ coating in subsequent experiment. According to the SEM images in Fig. 1d, the average thickness of $TiO_2$NPs was about 22.89 μm in 60 min of anodization.

### 3.2. Characterization of CuS@$TiO_2$NPs fiber

The morphology of the resultant CuS@$TiO_2$NPs nanocomposite was studied by scanning electron microscopy (SEM). As compared with the untreated Ti wire (Fig. 2a), the anodized fiber (Fig. 2b) shows that regular and dense $TiO_2$NPs are randomly oriented on the titanium substrate. After further high temperature annealing (Fig. 2c), the surface of the fiber became loose with defects, including holes, pores, microcracks by the reaction between OH groups on the surface of titanium dioxide particles. Notably, the surface of $TiO_2$NPs is smooth in Fig. 2b, however, which is interspersed with a large amount of small and well-dispersed nanoparticles in Fig. 2c. The surface area of coating increases greatly after $TiO_2$NPs annealed, and provides more reaction space for the subsequent generation of copper sulfide nanoparticles. Accordingly, from SEM images, we could observed clearly that the CuS nanoparticles grow uniformly on the surface of $TiO_2$NPs, forming the composite structure (Fig. 2d).

### 3.3. Surface composition

To find out the reasons for the high affinity of the fabricated fiber coating to the corresponding target analytes, the chemical composition of the Ti wire before and after treating was analyzed through energy dispersive X-ray spectroscopy (EDS). The surface of commercial titanium wire formed a very thin passivation layer due to long-term exposure in the atmosphere, so the spectral signals of very weak O elements can be seen from Fig. 3a. EDS analysis demonstrates the drastic increase in oxygen content with the increase of oxidation voltage and prolongation of oxidation time, at the same time the oxide films

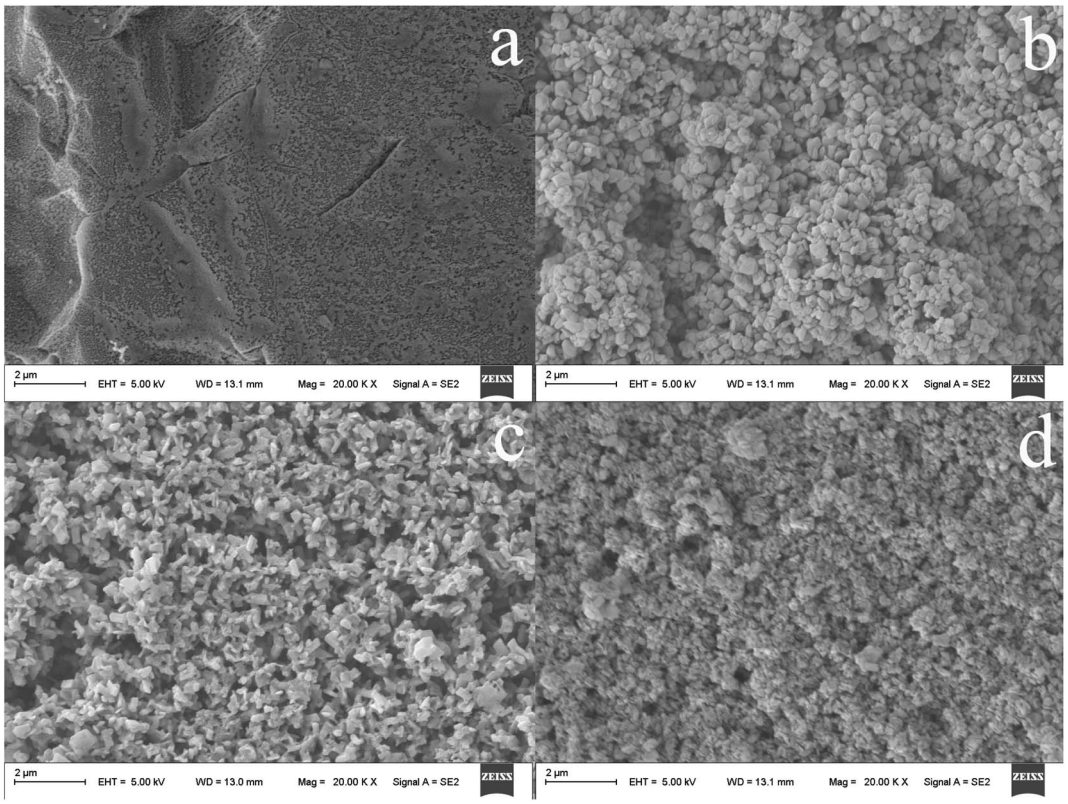


Fig. 2 SEM micrographs of the untreated Ti wire (a), the $TiO_2$NPs (b), the fiber obtained after annealed $TiO_2$NPs (c) and the CuS@$TiO_2$NPs/Ti coated fiber (d).

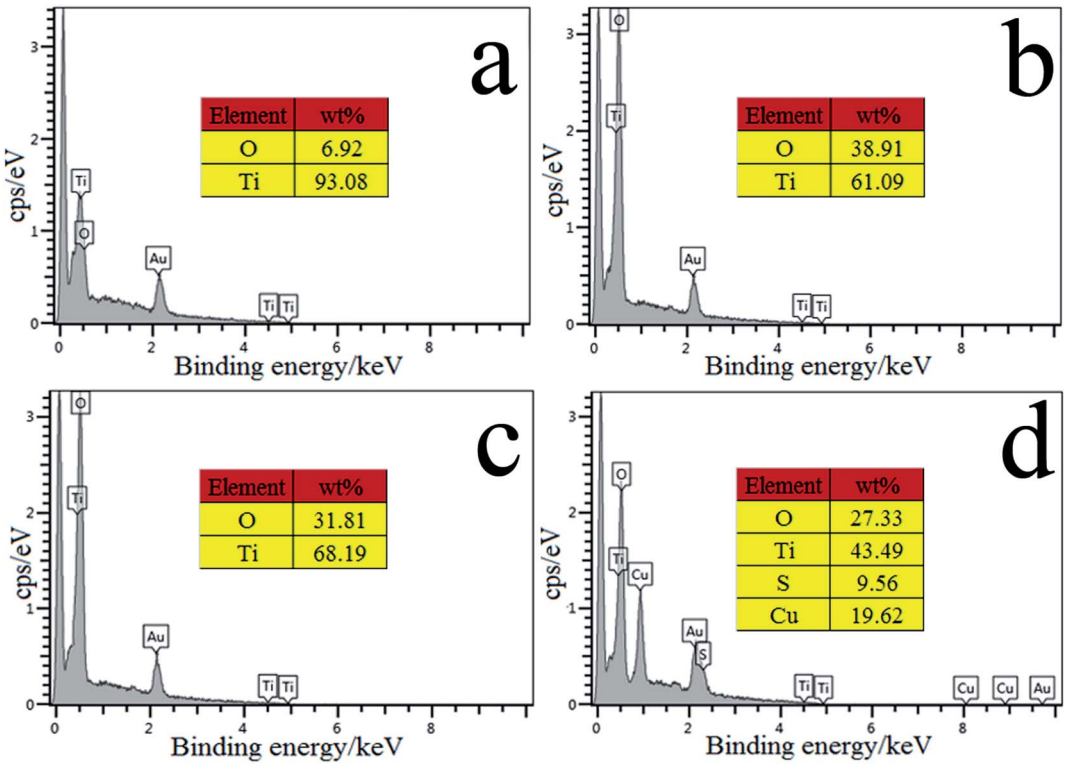


Fig. 3 EDS spectra of the untreated Ti wire (a), the $TiO_2$NPs (b), the fiber obtained after annealed $TiO_2$NPs (c) and the CuS@$TiO_2$NPs coated fiber (d).

deepens as well, O and Ti elements were more close to the $TiO_2$ element composition, the relative contents of Ti and O were 61.09% and 38.91%, respectively (Fig. 3b). As can be seen in Fig. 3c, the mass ratio of O and Ti remarkably decreases after anneal at 550 °C. It is indicated that the Ti–OH was destroyed by dehydration at high temperature annealed, resulted in the reduction of oxygen content (Fig. 3c). Further chemical deposition of CuS onto the $TiO_2$NPs coating surface results in considerable changes in the elemental composition. The signals of S and Cu elements are also observed at the same time (Fig. 3d). As can be seen in Fig. 3d, the content of O and Ti decreased while the content of S and Cu increased rapidly. Meanwhile, their mass composition was close to the composition molar ratio of $TiO_2$ and CuS compounds, it was a good illustration that $TiO_2$NPs have been doped with CuS nanoparticles.

### 3.4. Effects of annealing temperature

In order to enhance coating surface area and reactivity and improve compatibility for strong adhesion of CuS to the Ti fiber substrate. A series of $TiO_2$NPs/Ti fibers with different morphology and structure were prepared by annealing at 450 °C, 550 °C, 650 °C and 750 °C under nitrogen ambient, respectively. With the change of annealing temperature in a large range, the morphology and structure of $TiO_2$NPs coating changed obviously (Fig. 4). When the annealing temperature was 550 °C, the surface of $TiO_2$NPs becomes loose and small cracks appear, which was favourable to the chemical deposition of nano CuS. However, annealing temperature was further increased, the ordered level of the skeleton of $TiO_2$NPs were rapidly deteriorated due to its surface shrinkage (Fig. 3c and d). It is reported that anatase $TiO_2$ is mainly obtained by anodizing high-purity titanium at high oxidation voltage.[31] In addition, in general, the crystalline transform temperature of anatase $TiO_2$ to rutile $TiO_2$ was in the range from 610 °C to 915 °C.[32] The phase transition point of $TiO_2$ depends on the crystal size, within a certain range, the smaller the particle size, the lower the phase transition point, and the phase transition temperature of nanometer $TiO_2$ was 600 °C or lower.[33] Apparently, the crystal structure of $TiO_2$ changed during annealing. The oil absorption of rutile $TiO_2$ (16–48) was higher than that of anatase $TiO_2$ (18–30), while the Mohs hardness of rutile $TiO_2$ (6–7.5) was also higher than that of anatase $TiO_2$ (5.5–6). As a result, the change of morphology and strength of $TiO_2$NPs after high temperature annealing was beneficial to the modification and application of fiber coating. However the uniform frameworks of the $TiO_2$NPs composite coating were rapidly deteriorated and larger cracks produced at higher annealing temperature (Fig. 4c and d), which is not conducive to the surface doping of CuS. Based on the results in Fig. 4b, the optimized annealing temperature was confirmed as 550 °C for $TiO_2$NPs.

### 3.5. Effects of deposition cycle times

The annealed $TiO_2$NPs fiber coating was immersed in 1 mmol $L^{-1}$ $Cu(NO_3)_2$ solution for 10 min, washed with ultrapure water, and then immersed in 1 mmol $L^{-1}$ $Na_2S$ solution for 10 min, known as a deposition cycle. The solution of $Cu(NO_3)_2$ and $Na_2S$ with lower concentration and immersion method are used to

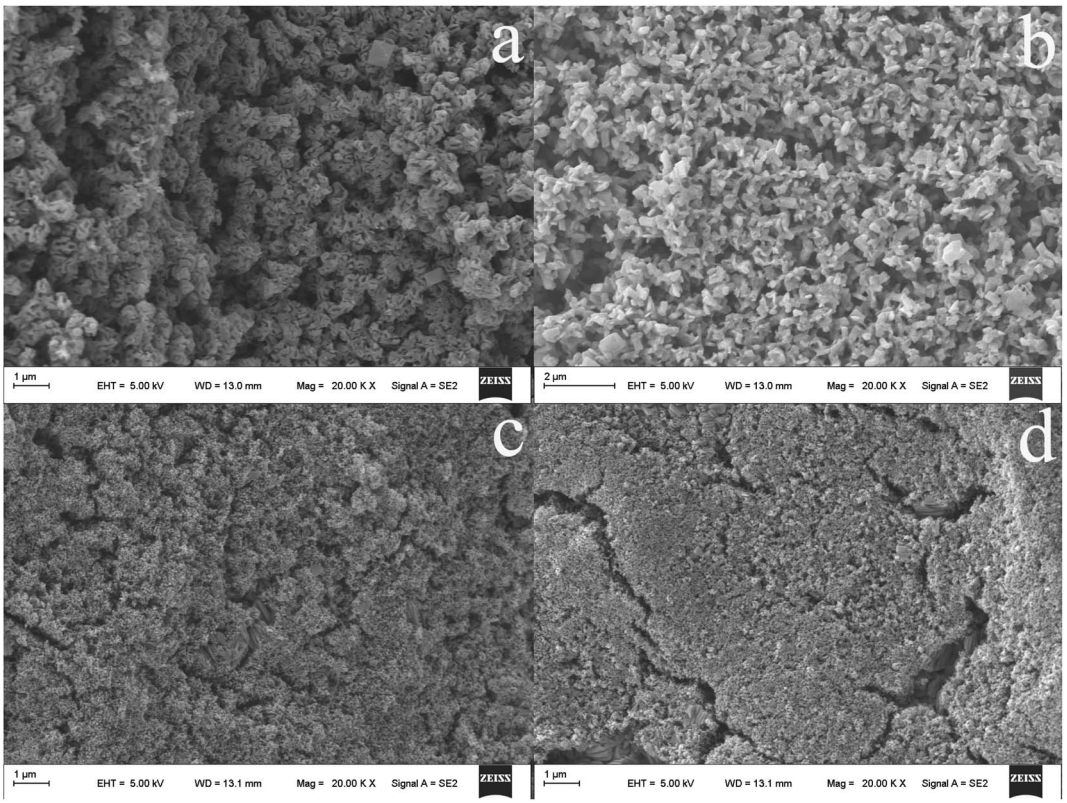


Fig. 4 SEM micrographs of the $TiO_2$NPs annealed at 450 °C (a), 550 °C (b), 650 °C (c) and 750 °C (d).

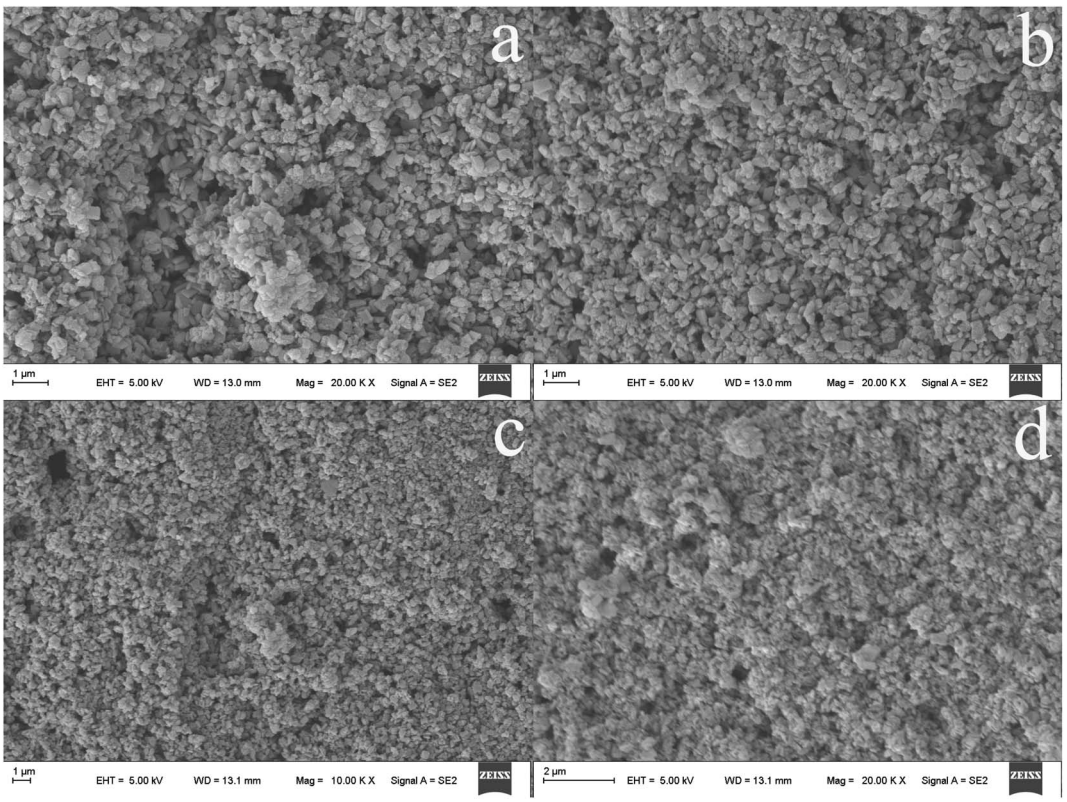


Fig. 5 SEM micrographs of the CuS@$TiO_2$NPs/Ti fibers prepared by dip-coating after 10 cycles (a), 15 cycles (b), 20 cycles (c) and 25 cycles (d).

prevent the formation of colloidal CuS. After several cycles, the fiber coating of CuS@$TiO_2$NPs was obtained. The number of cycles would change the composition of elements and the morphology on the surface of CuS@$TiO_2$NPs coating, and then affected the extraction efficiency of the coating. It can be seen from Fig. 5 that when the number of chemical deposition was 5 cycles, there are only a small amount of CuS nanoparticles. Along with the increase of deposition cycle number, the amount of CuS doping increases significantly. However, after the number of cycle exceeds 20, there was agglomeration and overlap phenomenon on the surface of the fiber coating, resulting in the disordered distribution of the mutually doped nanocomposite materials. Therefore, 20 cycles was the optimal deposition cycle.

### 3.6. Selectivity of CuS@$TiO_2$NPs/Ti fiber

The extraction efficiency and the selectivity of the CuS@$TiO_2$-NPs coating was further studied for SPME of aromatic amines (aniline, *p*-methylaniline, *p*-nitroaniline, diphenylamine), PAEs (DMP, DEP, DBP, DOP and DEHP), UV filters (BP, BP-3, OD-PABA, EHMC and EHS) and PAHs (Nap, Phe, Flt, Pyr and B[*a*]p) from aqueous phase.

It is noteworthy that the fiber exhibits excellent extraction selectivity for PAHs while almost no extraction capability toward aromatic amines and PAEs as shown in Fig. 6. This special extraction capability may be attributed to the inherent chemical natures of CuS@$TiO_2$NPs coatings. The surface doped fiber coating retained a large amount of $TiO_2$NPs structure. $TiO_2$ component in the CuS@$TiO_2$NPs composite coating may have Lewis acid sites on the coating surface, which provides the potential retention of non-polar PAHs and less polar UV filters through Lewis acid–base interaction. Due to the hydrophobicity of the $TiO_2$, the $TiO_2$NPs coating allows negligible extraction of polar aromatic amines and PAEs. CuS was immobilized on the surface of $TiO_2$NPs coating by postprecipitation, which enhanced the hydrophobicity of the coating and greatly enhanced the extraction effect of non-polar PAHs. Furthermore, the interaction between π electron of organic analyte and the microstructure of CuS@$TiO_2$NPs promoted the extraction of PAHs. Thus this new fiber was employed for selective SPME of PAHs in subsequent study.

### 3.7. Optimization of SPME conditions for PAHs

There are several parameters affecting the extraction performance such as extraction time, desorption time, temperature, stirring and ionic strength of sample solutions. Thus, to achieve the optimal extraction conditions, the details of various parameters on the extraction performance were studied as discussed in the following topics. The spiked concentrations of analytes were 25 mg $L^{-1}$ and all the experiments were conducted in triplicate and the means of the results were used for evaluation.

SPME is an equilibrium-based technique, and the equilibration time should be the optimum extraction time. The effect of extraction time on the extraction efficiency of target analytes was investigated in the range of 20–80 min. As shown in Fig. 7a,

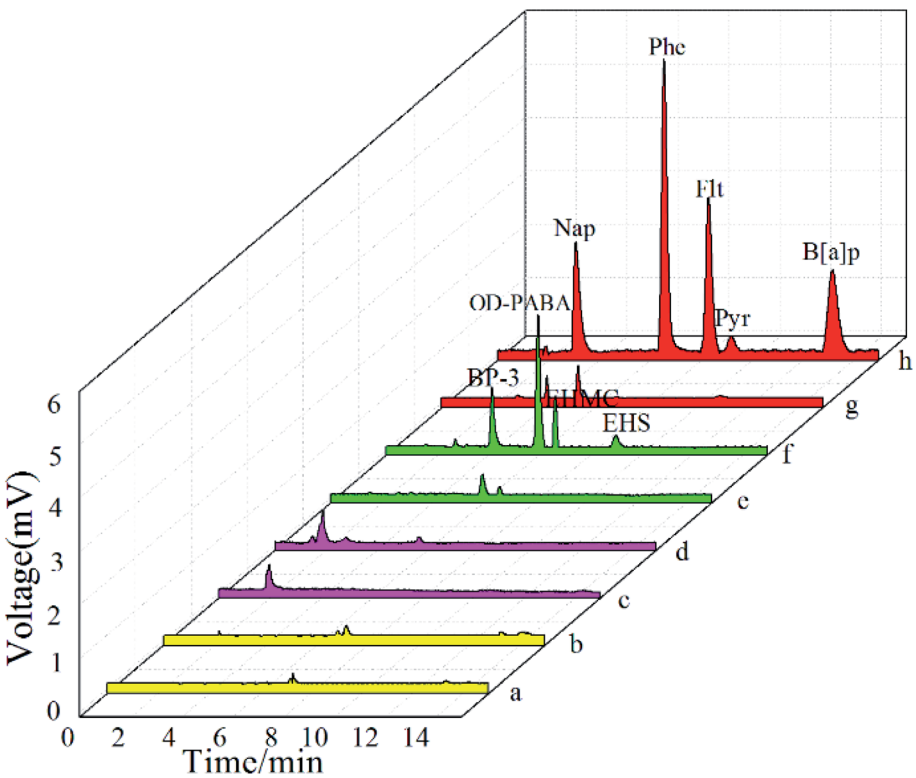


Fig. 6 Typical chromatograms of direct HPLC for aromatic amines (a), PAEs (c), UV filters (e) and PAHs (g) as well as corresponding SPME-HPLC with the CuS@$TiO_2$NPs/Ti fiber for aromatic amines (b), PAEs (d), UV filters (f) and PAHs (h). Extraction conditions: temperature, 40 °C; extraction time, 55 min; desorption time, 7 min; stirring rate, 300 rpm; analytes, 25 μg $L^{-1}$.

the extraction equilibrium was almost obtained for Nap, Phe and Pyr within 60 min but a longer time was needed to reach the extraction equilibrium of Flt and B[*a*]p. Considering only a slight increase in the peak areas of Flt and B[*a*]p after 60 min, 60 min is a reasonable compromise time between a good peak area and an acceptable extraction time for all PAHs. In order to achieve a high sensitivity and speed, the effect of desorption time was also studied by varying the time from 1 to 7 min. It was found that 3 min was adequate for the complete removal of the analyte from the fiber. Consequently, desorption time was selected as 3 min in further work.

The extraction temperature has positive and negative effects on extraction efficiency. In general, increasing temperature can enhance the mass transfer of analytes from the solution to the fiber coating. On the other hand, the partition coefficient between the fiber coating and the sample solution analyte will decrease with the increase of temperature. In addition, the effect of temperature on the extraction distribution ratios showed that all of the extraction reaction is exothermic reaction and high temperature is not beneficial to extraction. Fig. 7b presents the effect of temperature on the extraction of PAHs from 20 to 70 °C. The highest extraction efficiency is achieved at 50 °C and the extraction efficiency quickly decreases with further increase of temperature. Therefore, extraction temperature of 50 °C was chosen.

Stirring is significantly important because extraction is a dynamic diffusion-controlled process. The extraction efficiency is significantly affected by the stirring speed. It is generally accepted that the reduction of the diffusion layer is essential in order to reach equilibrium faster, which is easily achieved by sample agitation. In general, magnetic stirring is widely used in direct SPME process for agitation because it facilitates the mass transfer of the analytes between the bulk of the sample and the fiber. However more vigorously stirring leads to the formation of air bubbles around the fiber and is unfavorable for the adsorption of target analyte molecules onto the surface of the CuS@$TiO_2$NPs/Ti coating. Based on the results in Fig. 7c, 600 rpm maximum speed of stirrer was maintained for further studies.

Addition of salt into aqueous solution frequently causes a further decrease in solubility of the organic compounds in the water. The distribution coefficient of solutes increases and thus enhance their partitioning onto the fiber. On the other hand, addition of salt can increase the viscosity of aqueous solution, especially the solution at liquid–solid interface. This may limit their diffusion from bulk solution to the surface of fiber coating and contribute to lower extraction efficiency of studied compounds. In our study, the effect of ionic strength on extraction efficiency was investigated in the range of 0–30% (w/v). As shown in Fig. 7d, the extraction efficiency of target analyte increases with NaCl amount and reaches a plateau after 15% (w/v). In the further experiments, the optimum concentration of NaCl was fixed at 15%.

### 3.8. Analytical performance of the CuS@$TiO_2$NPs/Ti fiber in the extraction of PAHs

The analytical performance of self-made and commercially fiber was studied in order to explore their differences in selectivity for

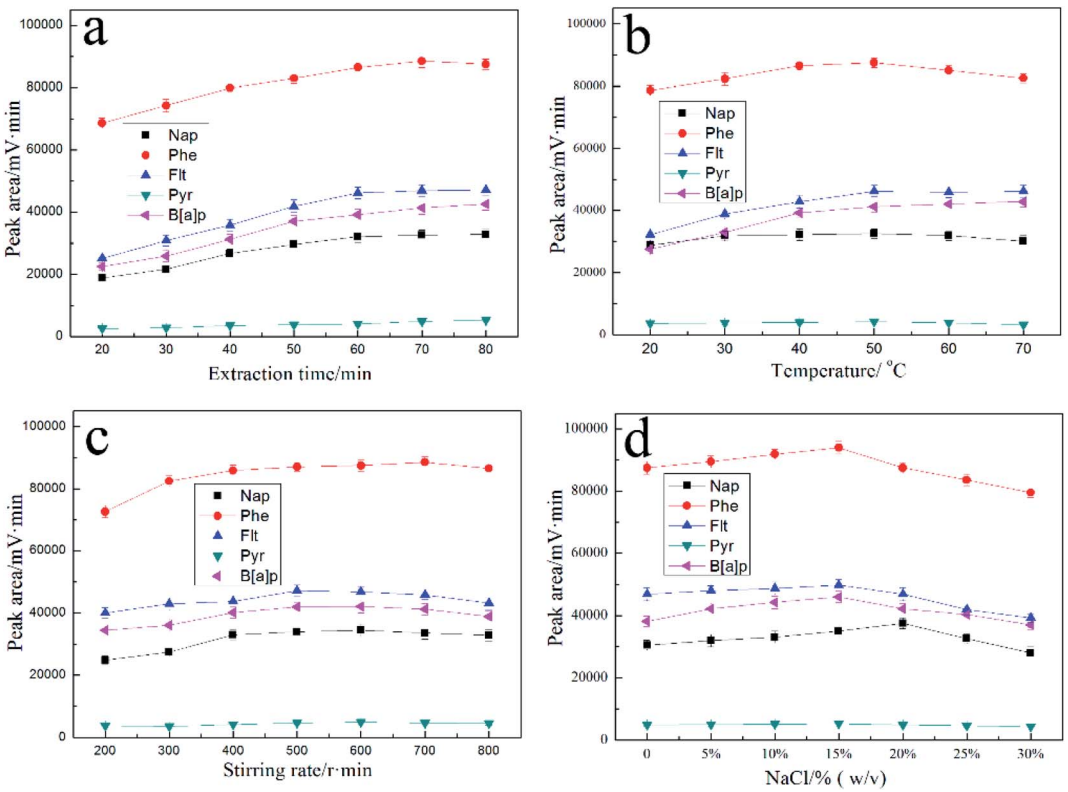


Fig. 7 Effect of extraction time (a), temperature (b), stirring rate (c) and ionic strength (d) on extraction efficiency.

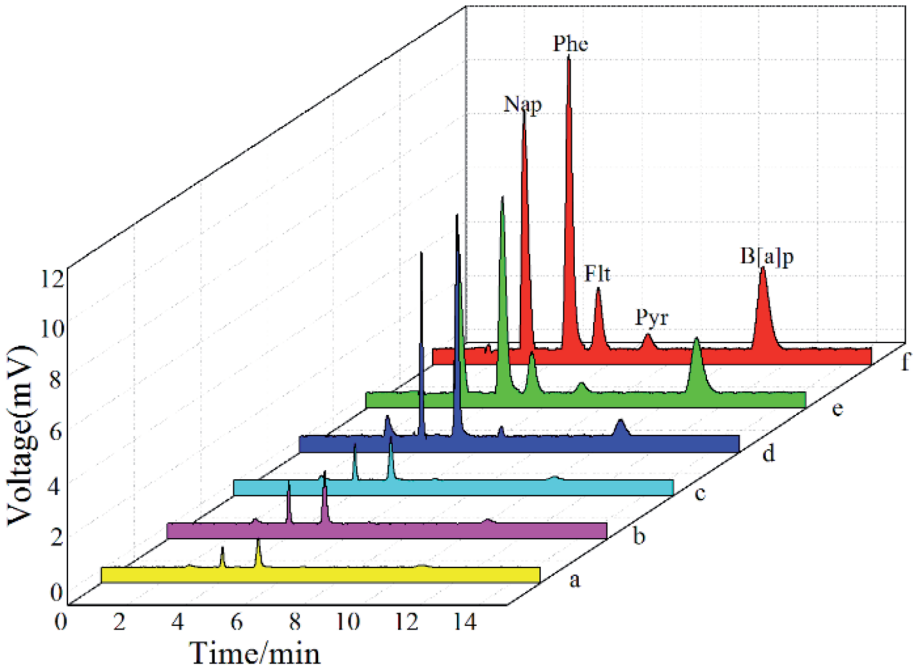


Fig. 8 Chromatograms of direct HPLC and SPME-HPLC for PAHs. Direct injection (a), SPME-HPLC with the untreated Ti wire (b), the 85 μm PA fiber (c), the $TiO_2$NPs/Ti fiber (d), the 100 μm PDMS fiber (e), the CuS@$TiO_2$NPs/Ti fiber (f) for PAHs spiked at 50 μg $L^{-1}$.

the PAHs. The extraction of PAHs was accomplished in the direct mode of SPME with each fiber under corresponding optimized conditions and the peak areas were compared (Fig. 8). According to these results, the CuS@$TiO_2$NPs/Ti fiber shows the best extraction efficiency for PAHs compared with Ti, $TiO_2$NPs/Ti, commercially available 85 μm PA and 100 μm PDMS fibers. The derivation of CuS doped nanostructure coating from annealed $TiO_2$NPs precursor is of great importance for its potential applications. Such a CuS@$TiO_2$NPs/Ti composite coating provides a potential alternative for selective extraction of PAHs from water samples.

The performance of the CuS@$TiO_2$NPs/Ti fiber in the extraction of PAHs in simulated wastewater samples was evaluated through obtention of the main analytical features under the optimized conditions described above (see Fig. S1†). The linearity, limits of detection (LODs), limits of quantitation (LOQs) and relative standard deviations (RSDs) were summarized in Table 1. Good linearity was achieved for all target analytes over the studied concentration ranging from 0.15 to 200 μg $L^{-1}$ with correlation coefficient ($R^2$) higher than 0.9913. The LODs and LOQs ranged from 0.02 to 0.04 μg $L^{-1}$ and from 0.07 to 0.13 μg $L^{-1}$ for PAHs based on the signal to noise ratio (S/N) of 3 and 10, respectively. The RSDs for the proposed method with the single fiber and the fibers fabricated in different batch varied from 3.2% to 4.3% and from 4.6% to 6.8%. It can be seen from the datum the proposed method exhibits excellent sensitivity, wide linear range and low detection limit, and the extraction effect of CuS@$TiO_2$NPs/Ti fiber on PAHs was better with low LODs and LOQs than that of $TiO_2$NTs fiber reported in literature.[34]

### 3.9. Spiked samples analysis

Hydrophobic PAHs are the most wide spread persistent organic pollutants and exist in various environmental water. They are of worldwide concern because some PAHs have some adverse

Table 1 Analytical parameters of the proposed method with the CuS@$TiO_2$NBs/Ti fiber ($n = 5$)

| PAHs | Linear equations[a] | Linearity (μg $L^{-1}$) | $R^2$ | Recovery[b] (%) | RSD[b] (%) | | LODs (μg $L^{-1}$) | LOQs (μg $L^{-1}$) |
|---|---|---|---|---|---|---|---|---|
| | | | | | Single fiber ($n = 5$) | Fiber-to-fiber ($n = 3$) | | |
| Nap | $Y = 460x + 1376$ | 0.15–200 | 0.9945 | 93.7 | 4.3 | 6.8 | 0.03 | 0.11 |
| Phe | $Y = 611x - 176$ | 0.15–200 | 0.9985 | 113 | 3.8 | 4.6 | 0.02 | 0.07 |
| Flt | $Y = 152x + 159$ | 0.15–200 | 0.9948 | 106 | 3.6 | 6.4 | 0.03 | 0.10 |
| Pyr | $Y = 50x + 134$ | 0.15–200 | 0.9923 | 107 | 3.5 | 5.7 | 0.04 | 0.13 |
| B[*a*]p | $Y = 314x + 1147$ | 0.15–200 | 0.9913 | 91.7 | 3.2 | 6.1 | 0.03 | 0.12 |

[a] $Y$, peak area; $x$, concentration of analytes. [b] Calculated at the concentration level of 50 μg $L^{-1}$.

effects on organisms, such as immunotoxicity, carcinogenicity and gene mutation, and have been proved to have the effect of environmental endocrine disruptors.

Lanzhou, Gansu Province, is located in the upper reaches of the Yellow River. The Yellow River passes through the city. At the same time, Lanzhou is densely populated and has many industrial and mining enterprises, including coal, petroleum, electric power, pharmaceutical and chemical industries. Lanzhou section is one of the sections with relatively serious pollution in the main stream of the Yellow River. At present, the pollutants in Lanzhou section of the Yellow River have changed from inorganic substances to organic substances, among which PAHs are one of the main organic pollutants. Due to the low solubility of PAHs in water, their concentration levels are very low in environmental water and thereby preconcentration is usually necessary before their efficient determination. Therefore, the established method was employed for selective preconcentration and determination of target PAHs in Yellow River water samples with the CuS@$TiO_2$NPs/Ti fiber, and the analytical results were summarized in Table 2. For the sake of examining the matrix effect and the accuracy of the proposed SPME-HPLC method, raw water samples spiked at two concentration levels were also used for recovery experiments in triplicate. As shown in Table 2, the relative recoveries for target PAHs were 82.1–115% at the spiking level of 5.0 μg $L^{-1}$ and 85.1–115% at the spiking level of 10.0 μg $L^{-1}$, respectively. Thus, the minor matrix effect is present in the SPME-HPLC procedure with the as-fabricated fiber. These results clearly demonstrate that the novel CuS@$TiO_2$NPs/Ti fiber is reliable and suitable for the selective preconcentration and determination of trace target PAHs in environmental water samples.

### 3.10. Stability and durability

In SPME, stability and durability is crucial for practical application of the SPME fiber. Damage of the coating was mainly caused by its exposure to high temperature, acidic or basic solution, and strong mechanical stirring during extraction processes. The single fiber used in this method showed no obvious decline in extraction efficiencies for PAHs after 200 SPME runs according to the prescribed experimental procedures. The recoveries ranged from 77.9% to 92.4% with the RSD between 5.1% and 8.1% was also obtained for five replicate analysis of spiked water with 50 μg $L^{-1}$. In order to examine its acid and alkali resistance, the fabricated fiber was allowed to be soaked in the solutions of 0.01 mol $L^{-1}$ $H_2SO_4$ and 0.1 mol $L^{-1}$ NaOH for 12 h. Negligible morphological changes were observed from its SEM image (see Fig. S2†), indicating that the fiber coating with perfect extraction performance was firmly immobilized to the CuS@$TiO_2$NPs/Ti fiber substrate with a rough surface structure and showed high stability towards acid, alkali and common organic solvents.

Table 2 Analytical results of PAHs in river water samples ($n$ = 3)

| | | | Spiked with 5 μg $L^{-1}$ | | | Spiked with 10 μg $L^{-1}$ | | |
|---|---|---|---|---|---|---|---|---|
| Water samples | PAHs | Original (μg $L^{-1}$) | Detected (μg $L^{-1}$) | Recovery (%) | RSD (%) | Detected (μg $L^{-1}$) | Recovery (%) | RSD (%) |
| River water under Bapanxia Bridge | Nap | 0.18 | 4.93 | 95.2 | 6.1 | 9.41 | 92.4 | 7.8 |
| | Phe | ND[a] | 5.18 | 104 | 5.8 | 11.46 | 115 | 6.9 |
| | Flt | ND | 5.19 | 104 | 6.5 | 11.54 | 115 | 7.4 |
| | Pyr | 9.12 | 14.48 | 103 | 6.7 | 20.05 | 105 | 8.0 |
| | B[*a*]p | 0.92 | 5.08 | 85.8 | 6.4 | 9.97 | 91.3 | 7.2 |
| River water under Yintan Bridge | Nap | 0.35 | 4.88 | 91.2 | 6.4 | 9.67 | 93.4 | 7.6 |
| | Phe | 0.83 | 6.12 | 105 | 5.4 | 11.87 | 110 | 6.5 |
| | Flt | ND | 5.34 | 107 | 6.2 | 11.23 | 112 | 7.3 |
| | Pyr | 4.39 | 10.21 | 109 | 6.8 | 16.32 | 113 | 7.7 |
| | B[*a*]p | 0.68 | 5.12 | 90.1 | 6.5 | 10.89 | 102 | 7.4 |
| River water under Zhongshan Bridge | Nap | 0.27 | 4.97 | 94.3 | 6.2 | 9.89 | 96.3 | 7.1 |
| | Phe | ND | 5.76 | 115 | 5.8 | 10.32 | 103 | 6.7 |
| | Flt | 0.94 | 5.45 | 91.8 | 6.5 | 9.88 | 90.3 | 7.4 |
| | Pyr | 2.54 | 8.56 | 114 | 7.0 | 14.15 | 113 | 8.1 |
| | B[*a*]p | ND | 4.15 | 83.0 | 6.4 | 8.96 | 89.6 | 7.9 |
| River water under Donggang Bridge | Nap | 0.34 | 5.02 | 94.0 | 6.4 | 8.99 | 86.9 | 7.2 |
| | Phe | 1.39 | 7.34 | 115 | 6.1 | 12.07 | 106 | 6.7 |
| | Flt | 1.20 | 5.31 | 85.6 | 6.3 | 10.06 | 89.8 | 7.4 |
| | Pyr | 1.39 | 7.03 | 110 | 6.9 | 11.98 | 105 | 7.6 |
| | B[*a*]p | 2.23 | 6.18 | 85.5 | 6.3 | 11.67 | 95.4 | 7.2 |
| River water under Sichuan Bridge | Nap | 0.20 | 4.27 | 82.1 | 5.8 | 9.66 | 94.7 | 6.7 |
| | Phe | 0.43 | 5.84 | 108 | 5.3 | 11.33 | 109 | 6.3 |
| | Flt | 2.18 | 6.32 | 88.0 | 5.1 | 10.76 | 88.3 | 6.2 |
| | Pyr | 4.68 | 10.72 | 111 | 5.3 | 15.92 | 108 | 6.8 |
| | B[*a*]p | ND | 4.55 | 91.0 | 6.0 | 8.51 | 85.1 | 6.9 |

[a] ND, not detected or lower than LOD.

## 4. Conclusions

Novel CuS@$TiO_2$NPs fibers were prepared by a simple electrochemical *in situ* anodic oxidation method on the Ti wire and subsequent the CuS nanoparticles was compounded onto $TiO_2$NPs by the method of postprecipitation. Due to its unique nanostructure, the robust fiber has a much larger surface area and more adsorptive sites exhibits greater extraction efficiency and betters electivity for the analytes, and is more effective than the commercially available PDMS and PA fibers. The proposed SPME-HPLC method using the new fiber showed good selectivity and sensitivity extract and separate target PAHs in aqueous solution and very low LODs were obtained. This fiber was used for more than 200 extraction and desorption cycles without the loss of the extraction capability. Thus, it is a promising alternative for use in SPME, being easily, reproducible and inexpensively prepared.

## Conflicts of interest

There are no conflicts to declare.

## Acknowledgements

This research work was financially supported by the Science and Technology Projects of Gansu Province (20JR10RA290), Key Talent Project of Gansu Province (2021) and Innovation Fund for Higher Education of Gansu Province (2021B-282) and State Key Laboratory of Environment-Friendly Energy Materials (KF-20-0217).

## References

1 É. A. Souza-Silva, R. F. Jiang, A. Rodríguez-Lafuente, E. Gionfriddo and J. Pawliszyn, A critical review of the state of the art of solid-phase microextraction of complex matrices I. Environmental analysis, *Trends Anal. Chem.*, 2015, **71**, 236–248.

2 S. Merkle, K. Kleeberg and J. Fritsche, Recent developments and applications of solid phase microextraction (SPME) in food and environmental analysis-a review, *Chromatography*, 2015, **2**, 293–381.

3 P. Berton, B. Lana, J. M. Ríos, J. F. Garcia-Reyes and J. C. Altamirano, State of the art of environmentally friendly sample preparation approaches for determination of PBDEs and metabolites in environmental and biological samples: a critical review, *Anal. Chim. Acta*, 2016, **905**, 24–41.

4 D. Fiorini and M. C. Boarelli, Solid-phase microextraction may catalyze hydrogenation when using hydrogen as carrier in gas chromatography, *J. Chromatogr. A*, 2016, **1453**, 134–137.

5 T. Fei, H. F. Li, M. Y. Ding, M. Ito and J. M. Lin, Determination of parabens in cosmetic products by solid-phase microextraction of poly(ethylene glycol) diacrylate thin film on fibers and ultra high-speed liquid chromatography with diode array detector, *J. Sep. Sci.*, 2015, **34**, 1599–1606.

6 A. R. Ghiasvand, S. Abdolhosseini, N. Heidari and B. Paull, Evaluation of polypyrrole/silver/polyethylene glycol nanocomposite sorbent for electroenhanced direct-immersion solid-phase microextraction of carvacrol and thymol from medicinal plants, *J. Iran. Chem. Soc.*, 2018, **15**, 2585–2592.

7 H. Bagheri, H. Piri-Moghadam and M. Naderi, Towards greater mechanical, thermal and chemical stability in solid-phase microextraction, *Trends Anal. Chem.*, 2012, **34**, 126–139.

8 M. Sajid, M. K. Nazal, M. Rutkowska, N. Szczepańska, J. Namieśnik and J. Płotka-Wasylka, Solid phase microextraction: apparatus, sorbent materials, and application, *Crit. Rev. Anal. Chem.*, 2019, **49**, 271–288.

9 S. Mohammad, J. M. Taghi and M. Mehdi, Carbon nanotubes@silicon dioxide nanohybrids coating for solid-phase microextraction of organophosphorus pesticides followed by gas chromatography-corona discharge ion mobility spectrometric detection, *J. Chromatogr. A*, 2016, **1429**, 30–39.

10 M. T. Jafari, M. Saraji and H. Sherafatmand, Polypyrrole/montmorillonite nanocomposite as a new solid phase microextraction fiber combined with gas chromatography–corona discharge ion mobility spectrometry for the simultaneous determination of diazinon and fenthion organophosphorus pesticides, *Anal. Chim. Acta*, 2014, **814**, 69–78.

11 F. Pena-Pereira, R. M. B. O. Duarte and A. C. Duarte, Immobilization strategies and analytical applications for metallic and metal-oxide nanomaterials on surfaces, *Trends Anal. Chem.*, 2012, **40**, 90–105.

12 M. G. Ma, H. J. Wang, Q. Zhen, M. Zhang and X. Z. Du, Development of nitrogen-enriched carbonaceous material coated titania nanotubes array as a fiber coating for solid-phase microextraction of ultraviolet filters in environmental water, *Talanta*, 2017, **167**, 118–125.

13 S. Zhao, S. Y. Wang, Y. Yan, L. Wang, G. S. Guo and X. Y. Wang, GO-META-$TiO_2$ composite monolithic columns for in-tube solid-phase microextraction of phosphopeptides, *Talanta*, 2019, **192**, 360–367.

14 S. Y. Wang, X. Y. Wang, L. Wang, Q. S. Pu, W. B. Du and G. S. Guo, Plasma-assisted alignment in the fabrication of microchannel-array-based in-tube solid-phase microextraction microchips packed with $TiO_2$ nanoparticles for phosphopeptide analysis, *Anal. Chim. Acta*, 2018, **1018**, 70–77.

15 D. D. Cao, J. X. Lv, J. F. Liu and G. B. Jiang, In situ fabrication of nanostructured titania coating on the surface of titanium wire: a new approach for preparation of solid-phase microextraction fiber, *Anal. Chim. Acta*, 2008, **611**, 56–61.

16 Y. Li, M. Zhang, Y. X. Yang, X. M. Wang and X. Z. Du, Electrochemical *in situ* fabrication of titanium dioxide-nanosheets on a titanium wire as a novel coating for selective solid-phase microextraction, *J. Chromatogr. A*, 2014, **1358**, 60–67.

17 M. G. Ma, H. J. Wang, M. Zhang, Q. Zhen and X. Z. Du, Facile fabrication of polyaniline coated titania nanotube arrays as

fiber coatings for solid phase microextraction coupled to high performance liquid chromatography for sensitive determination of UV filters in environmental water samples, *Anal. Methods*, 2016, **9**, 211–221.

18 X. M. Wang, H. Wang, P. F. Huang, X. M. Ma, X. G. Lu and X. Z. Du, Preparation of three-dimensional mesoporous polymer *in situ* polymerization solid phase microextraction fiber and its application to the determination of seven chlorophenols, *J. Chromatogr. A*, 2017, **1479**, 40–47.

19 M. Saraji, M. Ghani, B. Rezaei and M. Mokhtarianpour, Highly porous nanostructured copper foam fiber impregnated with an organic solvent for headspace liquid-phase microextraction, *J. Chromatogr. A*, 2016, **1469**, 25–34.

20 S. Mohammadiazar, A. Roostaie, M. Maghsoodi and M. Maham, Chemically deposited sol-gel film on porous $TiO_2$ nanotube arrays as an efficient and unbreakable solid-phase microextraction fiber, *Chromatographia*, 2018, **81**, 1–9.

21 L. Tao, Y. Xiong, H. Liu and W. Z. Shen, High performance PbS quantum dot sensitized solar cells *via* electric field assisted *in situ* chemical deposition on modulated $TiO_2$ nanotube arrays, *Nanoscale*, 2014, **6**, 931–938.

22 H. Wang, H. Y. Li, J. S. Wang, J. S. Wu, D. S. Li, M. Liu and P. L. Su, Nitrogen-doped $TiO_2$ nanoparticles better $TiO_2$ nanotube array photo-anodes for dye sensitized solar cells, *Electrochim. Acta*, 2014, **137**, 744–750.

23 H. Sun, P. N. Zhao, F. J. Zhang, Y. L. Liu and J. C. Hao, $Ag_2S$/CdS/$TiO_2$ nanotube array films with high photocurrent density by spotting sample method, *Nanoscale Res. Lett.*, 2015, **10**, 382–392.

24 K. Rajkumar, P. Vairaselvi, P. Saravanan, V. T. P. Vinod, M. Černík and R. T. R. Kumar, Visible-light-driven $SnO_2$/$TiO_2$ nanotube nanocomposite for textile effluent degradation, *RSC Adv.*, 2015, **5**, 20424–20431.

25 L. D. Sun, Y. Huang, H. A. Hossain, K. L. Li, S. Adams and Q. Wang, Fabrication of $TiO_2$/CuS CN bulk heterojunctions by profile-controlled electrodeposition, *J. Electrochem. Soc.*, 2012, **159**, 323–327.

26 Z. M. Wu, X. Tong, P. T. Sheng, W. L. Li, X. H. Yin, J. M. Zou and Q. Y. Cai, Fabrication of high-performance $CuInSe_2$ nanocrystals-modified $TiO_2$ NTs for photocatalytic degradation applications, *Appl. Surf. Sci.*, 2015, **351**, 309–315.

27 J. L. Qiao, Q. Y. Wang and Y. K. Xiao, High-efficiency photoelectrochemical performance of PbS nanoparticles sensitized $TiO_2$ nanotube arrays, *J. Appl. Electrochem.*, 2014, **44**, 1007–1011.

28 Y. Li, Y. X. Yang, H. X. Liu, X. M. Wang and X. Z. Du, Fabrication of a novel Ti-$TiO_2$-$ZrO_2$ fiber for solid-phase microextraction followed by high-performance liquid chromatography for sensitive determination of UV filters in environmental water samples, *Anal. Methods*, 2014, **6**, 8519–8525.

29 Z. Y. Wang, F. Y. Wang, R. Zhang, Z. Wang and X. Z. Du, A new strategy for electrochemical fabrication of manganese dioxide coatings based on silica nanoparticles deposited on titanium fibers for selective and highly efficient solid-phase microextraction, *New J. Chem.*, 2019, **43**, 5055–5064.

30 F. Rahmani, A. Es-Haghi, M. R. M. Hosseini and A. Mollahosseini, Preparation and characterization of a novel nanocomposite coating based on sol-gel titania/hydroxyapatite for solid-phase microextraction, *Microchem. J.*, 2019, **145**, 942–950.

31 D. W. Gong, G. A. Craig and V. K. Oomman, Titanium oxide nanotube arrays prepared by anodic oxidation, *J. Mater. Res.*, 2001, **16**, 3331–3334.

32 W. Y. Wu, Y. M. Chang and J. M. Ting, Room-temperature synthesis of single-crystalline anatase $TiO_2$ nanowires, *Cryst. Growth Des.*, 2010, **10**, 1646–1651.

33 G. H. Li, D. W. Wang, Z. D. Xu and W. X. Chen, Structure transition of nano-titania during calcination, *J. Cent. South Univ.*, 2003, **10**, 275–279.

34 H. M. Liu, D. A. Wang, L. Ji, J. B. Li and S. X. Jiang, A novel $TiO_2$ nanotube array/Ti wire incorporated solid-phase microextraction fiber with high strength, efficiency and selectivity, *J. Chromatogr. A*, 2010, **1217**, 1898–1903.